Combined dynamics of the 500–600 nm leaf absorption and chlorophyll fluorescence changes *in vivo*: Evidence for the multifunctional energy quenching role of xanthophylls

Shari Van Wittenberghe [a,b,*], Valero Laparra [c], José Ignacio García-Plazaola [d], Beatriz Fernández-Marín [e], Albert Porcar-Castell [b], José Moreno [a]

[a] *Laboratory of Earth Observation, Image Processing Laboratory, University of Valencia, C/ Catedrático José Beltrán, 2, 46980 Paterna, Valencia, Spain*
[b] *Optics of Photosynthesis Laboratory, Institute for Atmospheric and Earth System Research (INAR)/Forest Sciences, Viikki Plant Science Center (VIPS), University of Helsinki, PO Box 27, Latokartanonkaari 7, 00014 Helsinki, Finland*
[c] *Image and Signal Processing Group, Image Processing Laboratory, University of Valencia, C/ Catedrático José Beltrán, 2, 46980 Paterna, Valencia, Spain*
[d] *Department of Plant Biology and Ecology, University of the Basque Country (UPV/EHU), 48940 Leioa, Bizkaia, Spain*
[e] *Department of Botany, Ecology and Plant Physiology, University of La Laguna (ULL), 38200 La Laguna, Tenerife, Spain*

ARTICLE INFO

ABSTRACT

Carotenoids (Cars) regulate the energy flow towards the reaction centres in a versatile way whereby the switch between energy harvesting and dissipation is strongly modulated by the operation of the xanthophyll cycles. However, the cascade of molecular mechanisms during the change from light harvesting to energy dissipation remains spectrally poorly understood. By characterizing the *in vivo* absorbance changes (ΔA) of leaves from four species in the 500–600 nm range through a Gaussian decomposition, while measuring passively simultaneous Chl*a* fluorescence (F) changes, we present a direct observation of the quick antenna adjustments during a 3-min dark-to-high-light induction. Underlying spectral behaviours of the 500–600 nm ΔA feature can be characterized by a minimum set of three Gaussians distinguishing very quick dynamics during the first minute. Our results show the parallel trend of two Gaussian components and the prompt Chl*a* F quenching. Further, we observe similar quick kinetics between the relative behaviour of these components and the *in vivo* formations of antheraxanthin (Ant) and zeaxanthin (Zea), in parallel with the dynamic quenching of singlet excited chlorophyll *a* (^{1}Chl*a**) states. After these simultaneous quick kinetical behaviours of ΔA and F during the first minute, the 500–600 nm feature continues to increase, indicating a further enhanced absorption driven by the centrally located Gaussian until 3 min after sudden light exposure. Observing these precise underlying kinetic trends of the spectral behaviour in the 500–600 nm region shows the large potential of *in vivo* leaf spectroscopy to bring new insights on the quick redistribution and relaxation of excitation energy, indicating a key role for both Ant and Zea.

1. Introduction

The dynamics of the photosynthesis' light reactions are closely coupled to the controlled dynamics and interactions between chlorophyll (Chl) and carotenoid (Car) pigments, which has provided useful means to study the regulation of energy dissipation both *in vitro* and *in vivo*, from close range [1–3] to remote distances [4,5]. The photosynthetic pigments embedded in proteins forming the antenna complexes in all green plants and algae provide hereby a crucial function in the optimization of the flow of excitation energy towards the reaction centres (RC). By regulating this energy flow, the photosynthetic antennas exhibit a highly controlled dual role of light harvesting on the one hand, when excitation energy is effectively funnelled to the RC [6], and of photoprotection on the other hand, when excitation energy is dissipated as heat through the creation of energy sinks within the antenna [1,7].

The pertinent role of the Cars in the creation of these energy sinks has been shown based on several spectroscopic techniques indicating absorption changes in the light-harvesting antenna complexes. Cars are

excited by absorption of photons from wavelengths in the 350–550 nm range with, depending on the Car, differences in the absorption profile and functional role in the photosynthetic energy balance. While a light harvesting function has been demonstrated for violaxanthin [8–10], a role as energy quencher have been demonstrated for xanthophylls that activate upon a light-induced lumen acidification in what is known as the Violaxanthin-Antheraxanthin-Zeaxanthin or VAZ cycle [11]. Under light excess the quick built-up of a pH gradient (ΔpH) across the thylakoid membrane triggers the protonation of the PsbS protein and the activation of the violaxanthin de-epoxidase (VDE) that ultimately catalyses the inter-conversions in xanthophyll composition. Two xantho-phyll cycles have been described thus far in vascular plants: the VAZ cycle, ubiquitous in the subkingdom *Viridiplantae*, and the Lutein epoxide-Lutein (LxL) cycle, which is taxonomically restricted being present in approximately 60% of plant species analysed thus far [12,13]. Based on *in vitro* studies it is known that both VAZ and LxL cycles are triggered similarly and catalysed by the same enzymes [12], but oper-ating independently [14].

Despite these xanthophyll conversions seem well-understood, the *in vivo* energy regulation upon their formation and the various spectral behaviour during light adaptation remains unclear. Both *in vivo* and *in vitro* studies have observed specific absorption changes in the 500–600 nm region related to several mechanisms linked to the behaviour of xanthophylls [15–19], in addition to variable scattering behaviour from other processes such as chloroplast movement [20] or membrane rear-rangements [21], which complicate the designation of single-mechanism-features in the photosynthetic wavelength range [22]. Due to these dynamic and spectrally overlapping mechanisms, the associa-tion between xanthophyll(s) and specific absorption changes is still a challenging task. Further, several distinctive physical mechanisms or origins have been associated to specific 500–600 nm absorption features observed for quenched antenna states, hampering a clear consensus. Different mechanisms such as (1) a proton motive force-induced elec-trochromic shift feature of xanthophylls [23–25], (2) a newly allowed excitation transition of Cars [26], (3) the intersystem crossing of a Car from its singlet ($^1Car^*$) to its triplet ($^3Car^*$) state [27,28], or (4) a true electronic absorption change from a difference spectrum related to either a red-shifted zeaxanthin (Zea) [29] or violaxanthin (Vio) [15] have been proposed. The latter mechanism is further suggested to additionally involve a related conformational change accompanying the quenching process, triggered by the binding of the xanthophyll(s) to the antenna [30–32].

In the case of *in vivo* studies, the 500–600 nm leaf absorbance or reflectance changes have been related to the light-induced changes in VAZ composition both under sudden saturating light exposure in the time frame of a couple of minutes [16,18,33], and under natural diurnal increasing light conditions in the time frame of several hours [34,35]. Some additional influence of chloroplast motion has also been detected in the same spectral region, although this was often observed as slower increases in the overall scattering with a stronger effect in the 400–500 nm region [18,20,36]. Despite these overlapping spectral changes may potentially complicate an easy mechanistic understanding, the obser-vation of the specific changes in the 500–600 nm region are commonly used to remotely identify the photochemical pigment pool changes in vegetation reflectance [33,37]. More specifically, to derive the specific changes indicative for the de-epoxidation state of the photosynthetic antenna, the Photochemical Reflectance Index (PRI) was developed, a vegetation index based on the reflectance at 531 and 570 nm, which is commonly applied to gain understanding on the light use efficiency of leaves or vegetation surfaces. The PRI focusses on the changes of the peak wavelengths at 531 nm but wavelength-dependent behaviour in the 500–600 nm range has suggested possible multiple underlying mechanisms [16,38,39]. Slower (at approx. 515 nm) and faster (at approx. 555 nm) wavelengths have been detected in the reflectance or absorbance changes upon quick light saturation [39] but the mecha-nisms behind these changes are not clearly understood. Despite the

changes in the 500–600 nm region are clearly observed in the same time frame as the dynamic quenching of singlet excited chlorophyll-*a* ($^1Chla^*$) seen as fluorescence (F) quenching [22,40], the physical link between the xanthophyll dynamics, the energy quenching mechanisms and the absorbance changes remains unsolved. Dynamic quenching occurs due to the interaction of an excited state fluorophore (here $^1Chla^*$) with a quencher molecule resulting in the radiationless deacti-vation of the fluorophore to its molecular ground state. This decrease in F lifetime can be observed *in vivo* as the decrease in the emission during the Kautsky effect happening under a constant excitation. A large amount of experimental evidence demonstrates the involvement of antheraxanthin (Ant), Zea and lutein (Lut) as quencher molecules in the dynamic quenching mechanism of excited $^1Chla^*$ states [41–44], but the exact mechanism and the role of the different xanthophylls are still under debate [10,45–47].

In vivo leaf spectroscopy provides the possibility to study absorbance changes of photosynthetic active radiation, taking into consideration an adequate set-up in which an optic fiber with large enough field of view is used to measure the optical radiometric changes from both leaf sides [22]. The use of a low-pass filter, filtering incoming light above 650 nm, can moreover provide the possibility to simultaneously measure changes in spectral leaf-emitted Chl*a* F emission intensity [22,48]. Our proposed experiment, based on the measurement of high-spectral and high-temporal resolution absorbance changes during dark-to-high-light transients for leaves, aims to characterize the dynamic spectral behav-iour in the 500–600 nm range and to investigate its relation to xanthophyll conversions. By applying a Gaussian decomposition strat-egy for the 500–600 nm changes we examined if it was possible to: a) fit a minimum of Gaussians explaining the wavelength-dependent absorp-tion behaviour in this region, b) find consistent wavelength-specific trends, and c) understand the link between xanthophyll conversion behaviour, the 500–600 nm absorbance changes and the prompt $^1Chla^*$ quenching. Unravelling these key issues of quick energy regulation based on *in vivo* leaf spectra is essential to improve the spectral retrieval of vegetation dynamics to light excess from a proximal or even remote perspective.

2. Materials and methods

2.1. Transient reflectance, transmittance, absorbance and Chla F dynamics with a dual spectroradiometer set-up

Simultaneous leaf reflectance (R), transmittance (T) and Chl*a* F dark-to-high-light transient time series were measured in the spectroscopic laboratory for different species collected in the field. We selected the species *Morus alba* L. (white mulberry), *Juglans regia* L. (walnut), *Fagus sylvatica* L. (beech) and *Quercus robur* L. (pendunculate oak), with the latter known to have relatively high Lx content besides the ubiquitous VAZ pool. For each species branches and in the case of *Fagus sylvatica* L. (beech) whole seedlings were dark-adapted in the early morning. The branches were cut submerged in water at room temperature. After 2 h of dark adaptation single intact leaves attached to branches or to the whole plant were clipped inside the in-house designed FluoWat leaf clip [22,49,50] with two fiber optics, each connected to a spectroradiometer and inserted respectively in an upward and downward leaf clip opening. The fiber optic of an ASD FieldSpec full-range (400–2500 nm) spec-troradiometer (ASD Inc., Boulder, CO, USA) was inserted in the upper optical leaf clip opening (nadir position), while the second fiber optic of an ASD FieldSpec HandHeld 2 VNIR (325–1075 nm) spectroradiometer (ASD Inc., Boulder, CO, USA) was inserted in the bottom opening of the clip, both fibers pointing to the leaf surface under a FOV of 25°. This set-up allows simultaneous measurements of both upward and downward diffusely scattered leaf radiance ($L_{up}(\lambda, t)$, $L_{dw}(\lambda, t)$, W m^{-2} sr^{-1} nm^{-1}) with a spectral sampling of ±1 nm and a FWHM of <3 nm. The set-up is different from hemispherical measurements by measuring only under a 25° degree angle instead of the total hemispherical scattering. However,

since the light scattering at leaf surface level is merely determined by near-Lambertian L_{up} and L_{dw} components emanating from the leaf interior random multiple scattering, and surface properties are assumed constant during the transient, the changes (Δ) in scattered radiance allow to detect changes from the ensemble of leaf interior elements. The only error might be a slight underestimation of the calculated R or T, which does not affect the interpretation of the Δ measurements. This allows linking the leaf absorbance changes (ΔA) to specific absorption changes of the interior leaf elements. Inserting a 650-nm cut-off filter at the light opening of the leaf clip further allows the measurement of passively induced and spectrally resolved Chl$a$ F diffusively emitted from both leaf sides, $i.e.$ Fup(λ, t) and Fdw(λ, t), and measured in energy units W m^{-2} sr^{-1} nm^{-1}. We used two light sources in two comparable set-ups, $i.e.$ (1) a high-voltage single LED (High Cri LED 10 W 17 V 3050–5900 K, Yuji International Co., Ltd., Beijing, China), providing a 400–800 nm broadband radiation spectrum, and (2) a white LED panel (Photon System Instruments, s.r.o., Drásov, Czech Republic), providing a 400–780 nm broadband spectrum. Both illumination sources could be intensity controlled, providing an incoming LED irradiation of approx. 270 W m^{-2} (1200 µmol m^{-2} s^{-1}) in the PAR region (photosynthetic active radiation, 400–700 nm). For further details on the set-up, the reader is kindly referred to Van Wittenberghe et al. [22]. Spectral transients were collected for the dark-adapted leaves exposed to sudden and constant saturating light of approx. 1200 µmol m^{-2} s^{-1} with both spectroradiometers set to measure continuously single spectra for 5 min with an integration time of 136 (ASD FieldSpec) or 272 (ASD HandHeld) milliseconds. Due to a faster data acquisition of the HandHeld the integration time was set longer to obtain a data synchronization between the upward and downward radiance spectra. After each transient protocol a white spectral reference (Spectralon, Labsphere Inc., North Sutton, USA) was placed inside the leaf clip to measure the radiance received by the surface ($L_s(\lambda)$, W m^{-2} sr^{-1} nm^{-1}). Absorbance (A) time series were calculated as A = 1-R-T from the synchronic R and T time series obtained from the L_{up}, L_{dw} and L_s measurements. The transient series of $\Delta R(\lambda$, $t)$, $\Delta T(\lambda$, $t)$ and $\Delta A(\lambda$, $t)$ in the 500–600 nm range were obtained by subtracting the first measured spectrum (at $t = 0$ s) upon prompt illumination from the rest of the time series' spectra. To calculate the 3-min transient kinetic behaviour of each wavelength in the region, we calculated the normalized trend for each λ as the change through time divided by the maximal change until steady-state of the spectral changes at $t = 3$ min, $e.g.$ Norm $\Delta A(\lambda$, $t)$ = $\Delta A(\lambda$, $t)/\Delta A$max(λ, $t = 3$ min). The same was done for the Fup(λ, $t)$, Fdw(λ, $t)$ and Ftot(λ, $t)$ = Fup(λ, $t)$ + Fdw(λ, $t)$ signal changes at each wavelength in the 670–770 nm range to visualize the λ-dependent change in Chl$a$ F quenching relative to dark-adapted unquenched state at $t = 0$ min.

2.2. Xanthophyll and carotene conversions during dark-to-high-light transient

A leaf under a saturating high intensity illumination treatment typically reaches its maximal Zea pool (maximal de-epoxidation state) within approx. 10 min according to some references [16,29]. However, also shorter VAZ de-epoxidation conversion times of 2–3 min have been measured under a saturating light response [18]. Here, only the case of $Q. robur$ quick xanthophyll and carotene conversions were verified for 2 h-dark-adapted leaves. $Q. robur$ has a relatively high LxL pool when compared with most woody plants [51] which allowed us to simultaneously verify the VAZ and LxL conversion dynamics. Dark-to-light transient dynamics of these α- and β-branch xanthophylls and related carotene pools were measured by sampling two leaf disks of 6 mm diameter and subsequently exposing them to an LED at equal distance compared to the leaf clip set-up, providing saturating light of approx. 1400–1600 µmol m^{-2} s^{-1} during respectively 1, 10, 20, 30, 40, 60, 90, 120, 180 and 300 s, before freezing them immediately in liquid N$_2$. The same protocol was repeated twice during the first 3 min, each for a different leaf, including the sampling of unexposed dark-adapted disks.

Samples were stored at −80 °C until further pigment extraction. Cars and Chls were measured by reverse phase HPLC following the method described by García-Plazaola and Becerril [52]. Briefly, frozen leaf discs were extracted in pure acetone buffered with CaCO$_3$ and after centrifugation the supernatant was filtered through a 0.22 µm PTFE filter (Whatman, Maidstone, UK). Extracts were analysed in a Waters HPLC system equipped with a reverse-phased Waters Spherisorb ODS1 column and pigments were quantified using a PDA detector (Waters model 996) at 445 nm. Pigments were identified and quantified by comparison with pure standards.

2.3. Characterization of the in vivo 500–600 nm feature (ΔA, ΔR) by Gaussian peak (GP) decomposition

In solution, pigment absorption spectra are successfully described by a linear combination of Gaussian peak (GP) functions fitting the overall feature [53,54]. Considering the $\Delta A(\lambda$, $t)$ in the 500–600 nm region as an absorption-related change due to a chemical change in xanthophyll composition, we applied several fitting model strategies, all based on a decomposition by GPs. We applied these strategies on both the ΔA and ΔR leaf spectral transient datasets measured for the different species to detect wavelength-dependent tendencies in the features. Each transient dataset $D = \{x, Y\}$ used consists of a time series where x is the wavelength vector in the [490–590] nm range, and Y is the set of measured ΔR or ΔA during the 3-min transient (Section 2.1), where we have a vector of measures $y^{(t)}$ per each time step t, $i.e.$ $Y = [y^{(1)} \ldots y^{(T)}]$, being T the number times the ΔA or ΔR were measured during the 3-min transient. We used a multiple Gaussian peak model to describe the ΔA or ΔR data given by:

$$f^{(t)}(x) = \sum_{i=1}^{N_g} a_i^{(t)} exp^{-\left(\frac{x-b_i^{(t)}}{c_i^{(t)}}\right)^2},$$

where N_g is the number of GPs. Hence, for each time step t we fit a different model $f^{(t)}(x)$ with N_g sets of three parameters for each Gaussian i: the weight ($a_i^{(t)}$), the mean ($b_i^{(t)}$), and the standard deviation (σ)-related ($c_i^{(t)}$), with $c = \sqrt{2}*\sigma$. To obtain the parameter sets we perform a fitting procedure consisting on the parameter domain search minimizing the mean square error between the real values $y^{(t)}$ and the values predicted by the model $f^{(t)}$:

$$\left[a_i^{(t)}, b_i^{(t)}, c_i^{(t)}\right] = argmin_{a,b,c} \sum \left(f^{(t)}(x) - y^{(t)}\right)^2$$

The solution obtained by the fitting procedure is highly dependent on the initial parameters and the restrictions imposed over the iterative solution. The adequate number of Gaussians N_g to explain the wavelength-dependent variation in the ΔR and ΔA changes is unknown, but multiple Gaussians can be considered from a theoretical point of view considering VAZ conversion dynamics (Fig. 1). $In vitro$ normalized absorption of the VAZ pigments indicate a strong peak overlap in the 400–500 nm region (Fig. 1a), giving maximal absorbance differences in the 470–520 nm tail region (Fig. 1b). Both Vio → Ant and Ant → Zea conversions show two main positive difference peaks increasing the net absorption. Assuming only an electrochromic shift between $in vitro$ and $in vivo$ absorption features, four positively weighted Gaussians could theoretically be considered. The inclusion of a negatively weighted Gaussian could additionally be considered. However, due to the strong possible overlap of these features, a lower N_g might statistically provide an adequate fitting.

We explored three different fitting strategies, from less to more constrained approaches. First, we apply an unconstrained fitting and determine a range of possible number of Gaussians for the model. Besides the number of Gaussians, in the second fitting strategy we impose a minimum set of physical restrictions to improve the detection of the underlying mechanisms. The main goal of this second strategy is to find
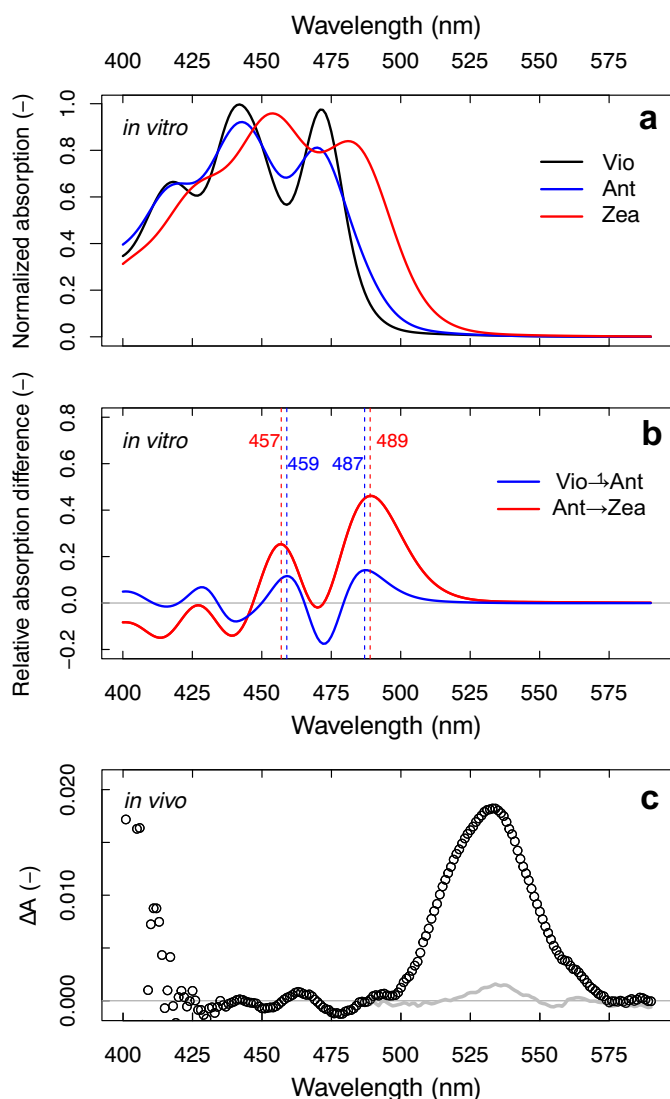
Fig. 1. *In vitro* (acetone) absorption spectra due to the S_0–S_2 electronic transition of the VAZ pool pigments (after Küpper et al. [54], see Appendix A, Table S1), normalized to the maximal absorbance peak of Vio and the relative absorption coefficients for Ant and Zea in acetone applied (a), and the simulated *in vitro* difference spectra for the conversion Vio → Ant and Ant → Zea, with the corresponding peak locations (b). In comparison, a steady-state absorbance difference (ΔA) profile *in vivo* measured with a dual spectroradiometer set-up with a *M. alba* leaf showing the difference between the dark- and light-adapted state after 3 min of light exposure (c).

a fixed set of parameters $[b_i^{(t)}, c_i^{(t)}]$ which we set in the third fitting. In this last fitting the only free parameter are the weights of the GPs, that we fit in each time step to uncover dynamics of the underlying spectral behaviour.

2.3.1. Unconstrained fitting by multiple Gaussians decomposition

To define the number of Gaussians statistically required for a good fitting of the ΔR and ΔA differential transient features, we applied a purely random (besides $b_i^{(t)} > 0$) fitting using two to eight GPs. In a preliminary round we evaluated the unconstrained fitting also through time for six leaves considering only two and three Gaussians (Fig. 2a–b). We observed poor random fitting results in the first minute of the transient, showing normalized errors exceeding 10% which can be explained by rather unstable differential features at the transient beginning requiring a higher N_g. To keep the models as simple as possible the N_g should be kept low. Also, to appreciate better the relative
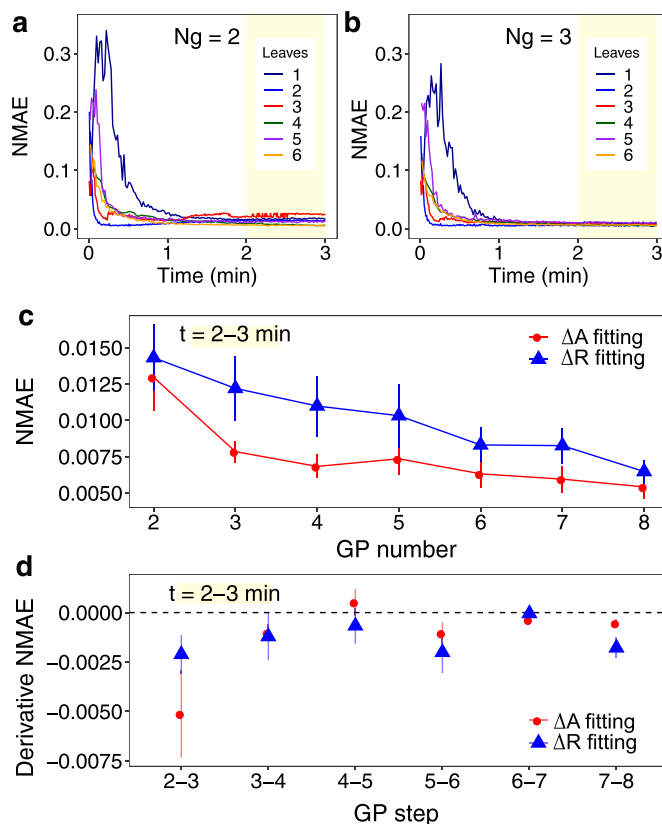

Fig. 2. Normalized fitting error (NMAE) for the unconstrained fitting of the 500–600 nm ΔA feature using 2 (a) and 3 (b) Gaussians peaks (GP) during the 3-min spectral transient of six leaves (*M. alba*: 1, 2; *F. sylvatica*: 3, 4, 5; *J. regia*: 6). A subset of the species-pooled ΔR (blue triangles) and ΔA (red bullets) transient series ($t = 2$–3 min, yellow marked) was further used to calculate the NMAE and its derivative (±SE, $n = 230$) for fitting scenarios with $N_g = [2$–8] (c, d) in order to evaluate the relative fitting improvement when including an additional GP. (For interpretation of the references to colour in this figure legend, the reader is referred to the web version of this article.)

fitting improvement when including an additional GP for the steady-state feature of different species we tested the unconstrained fitting only for the last minute of the transient, focusing in general on the steady-state shape (Fig. 2c–d). An increasing N_g obviously improved the fitting, but the relative improvement became negligible after a certain number. For the ΔA feature, a considerable improvement was found from the derivative between $N_g = 2$ and $N_g = 3$, with slight improvement for $N_g = 4$. No further improvement was found using $N_g = 5$, wherefore we constrained the test cases for the ΔA fitting to $N_g = [3,4]$. For the ΔR fitting, a relative improvement was found until $N_g = 8$, but at $N_g = 5$ the normalized mean absolute error (NMAE) was found below 1% which was considered a good fit (Fig. 2c). Hence, for the ΔR time series the cases $N_g = [3,4,5]$ were further tested.

2.3.2. Constrained Gaussian fitting with time coherence

Besides the constraining set of N_g, we explored further restrictions in the search space of the other parameters involved in the model. To constrain the randomness in the parameter search we enforced the coherence between the model parameters $[a_i^{(t)}, b_i^{(t)}, c_i^{(t)}]$ consecutive in time by initializing the search of the parameters in each time step with the parameters found in the previous time step. Further we tested the inclusion of an additional Gaussian in the central spectral range [510, 540] nm to describe a possible negative contribution in the differential features (Fig. 1b). For this, we allowed the N_g range to be extended by one additional GP, *i.e.* giving respectively $N_g = [4,5]$ and $N_g = [4,5,6]$ for the ΔA and ΔR data sets.

To avoid fitting too much overlap of the underlying mechanisms we also avoided the use of very broad Gaussians. For constraining the $c_i^{(t)}$ we observed the characteristics of the *in vitro* absorbance features (Fig. 1a) described by single Gaussians according to Küpper et al. [54] as shown in Table S1 (Appendix A). The standard deviations of the Gaussians in the red-sided tail leading to the difference feature are respectively 10.76 nm (Vio), 11.71 nm (Ant) and 15.54 nm (Zea), while the features resulting from their spectral difference (Fig. 1b) could be described by Gaussians as well. We performed a fitting of these features and found standard deviations of respectively 3.88 (Vio → Ant, peak max 459 nm), 7.43 (Vio → Ant, peak max 487 nm), 4.99 (Ant → Zea, peak max 457 nm) and 10.21 (Ant → Zea, peak max 489 nm) nm indicating possible constraints for $c_i^{(t)}$. However, for the *in vivo* fitting we allowed the $c_i^{(t)}$ parameter to extent until 15 nm considering possible effects of the (unknown) *in vivo* electromagnetic field conditions. To explain as much of the physically underlying behaviour as possible we restricted the distance of the centres of the positive Gaussians to be >50 nm/N_g. The negative GP was only restricted in the [510, 540] range. Further, the weight for each Gaussian was restricted by the maximum value of the measure, *i.e.* $a_i^{(t)} < max\ y^{(t)}$. We run this constrained fitting model for the ΔA ($n = 425$, 7 leaves) and ΔR ($n = 555$, 9 leaves) datasets. Based on the highest abundance of the values in the parameter set $[b_i^{(t)}, c_i^{(t)}]$ we defined the final model (Appendix A, Table S2).

2.3.3. Final fitting of the ΔA and ΔR transient feature

The final models were fitted using the restrictions of previous Sections 2.3.1 and 2.3.2 for the sets of N_g, without and with the negative Gaussian. The fixed sets of $[b_i^{(t)}, c_i^{(t)}]$ for each model was applied for the full 3-min transient, varying only the weights, $a_i^{(t)}$. To quantify the

relative importance of the absorption given by each Gaussian we normalized the integral of the Gaussians to 1, resulting in a weight $\frac{a_i}{c_i \sqrt{2\pi}}$. The relative magnitude of each normalized Gaussian in the overall feature, presenting the importance of each mechanism, was calculated through time as

$$Norm\ a_i^{(t)} = \frac{\frac{a_i^{(t)}}{c_i^{(t)}}}{\sum_i^{N_g} \frac{a_i^{(t)}}{c_i^{(t)}}}$$

where the term $\sqrt{2\pi}$ of the weight is cancelled out.

3. Results

3.1. VAZ (and LxL) dynamics and 500–600 nm ΔA during dark-to-high-light transition

During exposure to high light intensity of dark-adapted leaves, both leaf R and T factor changes in the 500–600 nm range show an decrease in equal magnitude for all species tested (typically 1% of each factor at 535 nm) indicating a true ΔA increase related to a change in chromophore composition. When avoiding leaves that show a strong effect of chloroplast movement, *i.e.* expected to be seen as more wide features over the full 400–700 nm range, we are able to detect this bell-shaped specific ΔA feature in the 500–600 nm range without any further spectrally overlapping mechanism. An example is given in Fig. 3 for a *M. alba* leaf showing the bell-shaped feature in the PRI-region. Simultaneous light-induced quenching of Chl*a* Fup(λ, t) and Fdw(λ, t), together with their sum Ftot(λ, t), are shown (Fig. 4). For both the
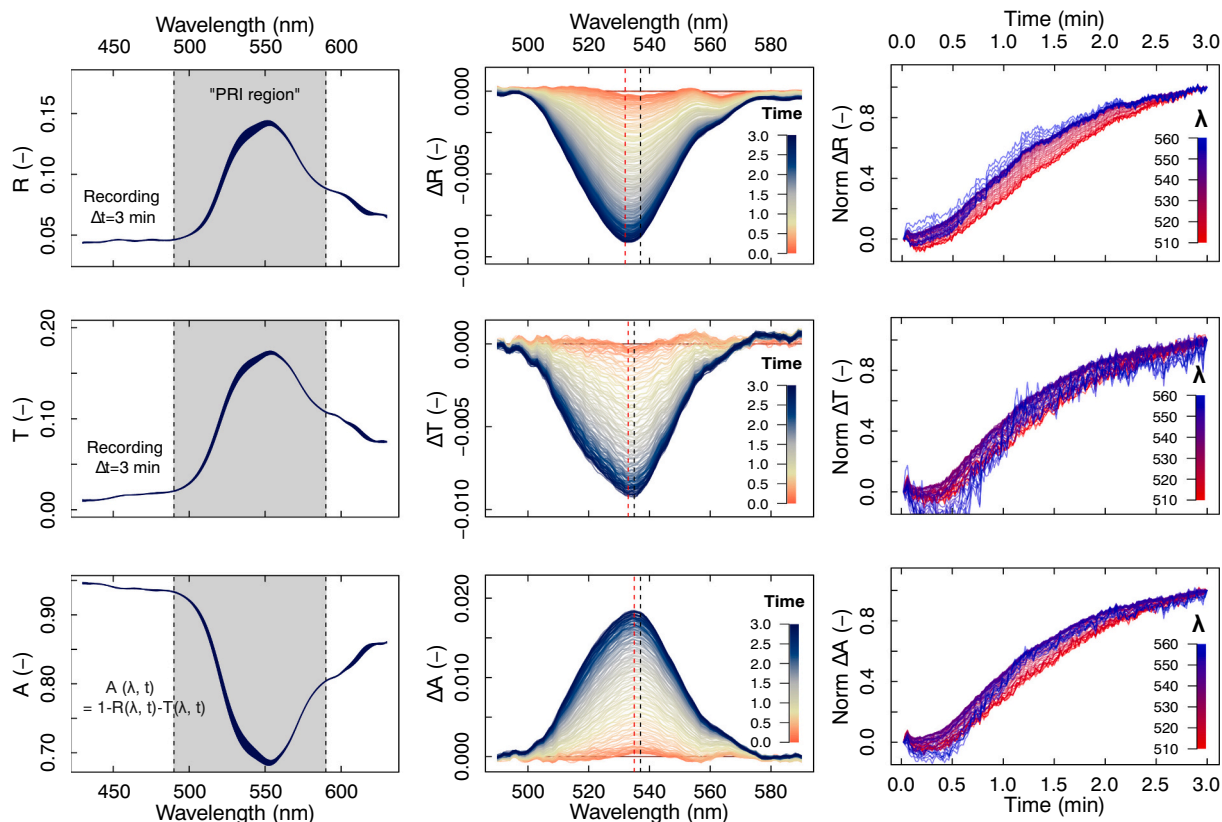

Fig. 3. Left column: Reflectance, transmittance and absorbance (R, T, A) spectra of a *M. alba* leaf shown superimposed from the dual spectroradiometer set-up during a 3-min continuous recording of a sudden dark-to-high light intensity exposure (approx. 1300 μmol m^{-2} s^{-1}). Middle column: ΔR and ΔT decreases and ΔA increases in the 500–600 nm range with the peak maxima location at the start (black dashed line) and the end (red dashed line) indicated. Right column: normalized trend of ΔR, ΔT and ΔA for each λ as the change through time (all presented positive) divided by the maximal change until steady-state at $t = 3$ min. (For interpretation of the references to colour in this figure legend, the reader is referred to the web version of this article.)
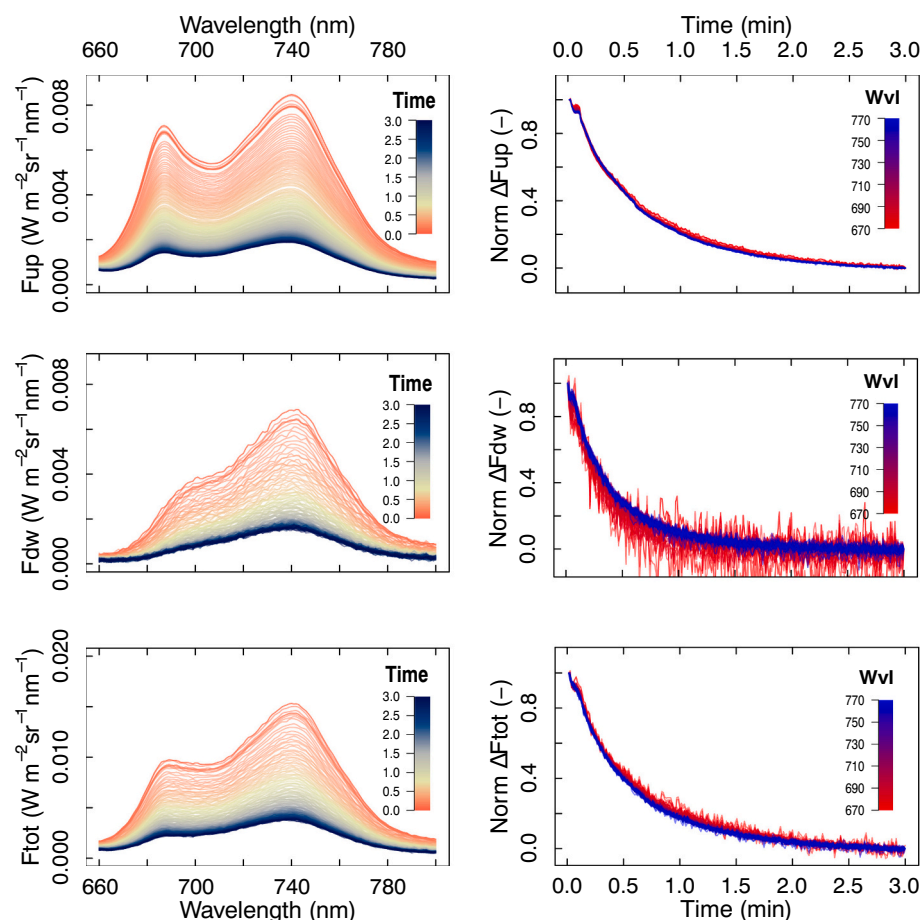
Fig. 4. Left column: Decreasing leaf-emitted Chl*a* fluorescence F (λ, *t*) from the dual spectroradiometer set-up of a *M. alba* leaf upon a 3-min dark-to-high-light intensity exposure (approx. 1300 µmol m^{-2} s^{-1}) showing the emission from the adaxial (Fup) and abaxial (Fdw) leaf surface, and their sum (Ftot). Right column: kinetic trend of each F wavelength in the 670–770 nm range during the dynamic quenching presented as the normalized F decrease relative to F at *t* = 0 min and divided by the maximal change at Δt = 3 min.

510–560 nm (ΔR, ΔT, ΔA) and the 670–770 nm (ΔFup, ΔFdw, ΔFtot) changes, the normalized trend of each wavelength during the 3-min transient is shown, illustrating the speed of the spectral change until steady-state at *t* = 3 min is reached. For the Norm ΔR, ΔT, ΔA changes a λ-dependent transient change can be noticed (Fig. 3) while for the Norm ΔFup, ΔFdw, ΔFtot changes the evolution through time appears rather λ-independent (Fig. 4). Hence, the wavelength behaviour in the 500–600 nm region indicates multiple underlying mechanisms which are not necessarily synchronized with the observed F changes given the faster overall trend of the latter.

The transient evolution in Car pools of *Q. robur* sun leaves are presented normalized to the stable Chl*a* pool (verified as [total Car/Chl*a*] = 0.47 ± 0.02 mol mol^{-1}, *n* = 31) in Fig. 5 indicating the molecular changes of both the α-branch and β-branch Cars during 5 min. The β-branch xanthophyll pools show a quick de-epoxidation of Vio during the first 30 s. To derive the rate constant k of the Vio de-epoxidation an exponential function was fitted representing the first-order reaction kinetics of the [Vio/Chl*a*] trend:

$$[Vio/Chla] = [Vio/Chla]_s + [Vio/Chla]_c * e^{-kt}$$

With [Vio/Chl*a*]$_s$ representing the proportional steady-state [Vio] pool which does not convert during the transient, and [Vio/Chl*a*]$_c$ being proportional to the convertible [Vio] pool, *i.e.* [Vio/Chl*a*]$^{t=0}$ minus [Vio/Chl*a*]$_s$ (Fig. 5). By fitting this reaction equation to our single example, we derive a Vio de-epoxidation rate constant k = 1.938 min^{-1}. Relative contributions of Ant, Zea and Neo formation from the Vio conversion during the first 30 s are shown in Fig. 6a, demonstrating a similar quick molecular formation of Ant and Zea. After 30 s, further Zea formation takes place until a maximal value is reached at *t* = 2 min, together with an observed decrease in β-Car. The α-branch pool shows a

quick rise in Lx within the same time frame as Ant formation, giving maximal values at *t* = 20 s, followed by a similar slow decrease (Fig. 5). Apart from the VAZ and LxL xanthophylls, further dynamics are seen in β-Car (slow decrease) and α-Car (slow increase) during the first minutes.

3.2. Gaussian decomposition of the ΔA (and ΔR) feature and transient behaviour

Decomposition of both the ΔA and ΔR differential feature into multiple Gaussians showed very good fitting results for all fixed sets of $[b_i^{(t)}, c_i^{(t)}]$ for each tested model (see Appendix A, Table S2). Generally, fitting for the set of constraints and selected N_g range showed good results with NMAEs >1% in only few cases. Constraining the standard deviation of the peaks to 15 nm to avoid very broad peaks probably eroded the fitting results only slightly compared to the random fittings. The forced inclusion of a negatively weighted Gaussian did not improve the ΔA feature fitting compared to an equal amount of total N_g without this forcing and did only slightly for the ΔR models (see Appendix A, Table S2). Moreover, in two cases of the forced negative GP fitting (Absorbance, N_g = 5; Reflectance, N_g = 5) the standard deviation for the Gaussian was zero, giving no statistical requirement of this feature.

With the major objective to keep the model as simple as possible we present in detail the ΔA feature decomposition by three positive Gaussians (N_g = 3, without negative GP, NMAE = 1.73 ± 0.59%) for three species in Fig. 7 (for comparison more complex models based on ΔR are shown in Appendix A Fig. S1). Gaussian decomposition of this simplest constrained model is based on three GPs with respective centres at 513.0 (GP1), 535.4 (GP2) and 563.3 (GP3) nm, all using a standard deviation of 15 nm. The steady-state feature at *t* = 3 min is shown with the final GP decomposition while the dynamic evolution of the weights
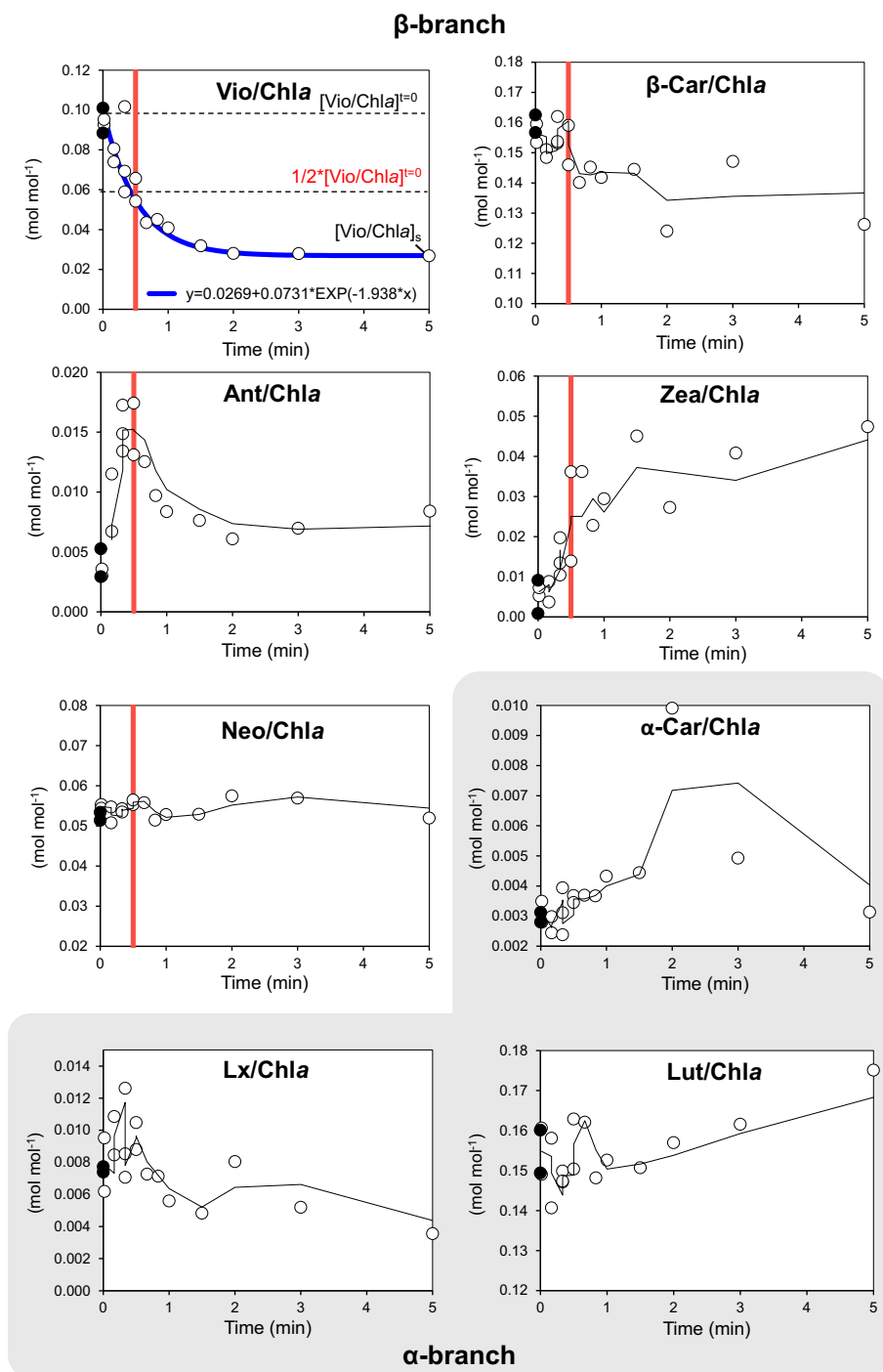
Fig. 5. α- and β-Car branch pool composition normalized to Chl*a* (mol mol^{-1}) of *Q. robur* leaves before (dark-adapted, black bullets) and during (Δ*t*-exposed, white bullets) acclimation to saturating illumination (approx. 1600 μmol m^{-2} s^{-1}). The 3-step moving average is plotted to illustrate the dynamic trends while the Vio de-epoxidation is presented by an exponential function considering a steady-state pool [Vio/Chl*a*]$_s$. The vertical red line at *t* = 30s coincides with the half-time of Vio/Chl*a* decrease (as proxy for [Vio] decrease) and the peak of Ant formation. (For interpretation of the references to colour in this figure legend, the reader is referred to the web version of this article.)

and the normalized weights are illustrating the GP behaviour through time. An example with spectral fitting results for different transient time intervals is given in Appendix A, Fig. S1.

3.3. Chla F quenching and GP component behaviour during xanthophyll conversion

In case the Gaussian peak fitting performs well during the early stage of the transient (*t* = 0–1 min), quick spectral dynamics can be distinguished from the sudden *Norm* $a_i^{(t)}$ trends upon illumination. In the examples shown for a *F. sylvatica* (middle) and *J. regia* leaf (right) in Fig. 7 a quickly developing relative importance of the central Gaussian (GP2 535.4 nm, *Norm* $a_2^{(t)}$) takes place reaching a maximum at *t* = 30 s or

sooner, followed by a relative decrease due to an increasing importance of the Gaussian in the shorter λ tail (GP1 513.0 nm, *Norm* $a_1^{(t)}$). This Gaussian peak starts increasing around *t* = 30 s, and reaches a maximum relative weight *Norm* $a_1^{(t)}$ around *t* = 2 min. The normalized weight of the third Gaussian (GP3 563.3 nm) in the longer λ tail indicates the summarized countereffect of both increasing components GP2 and GP1. These consistent underlying behaviours are also observed for the fittings applied on the ΔR changes including more complex models (see Appendix A, Fig. S1). Further, the *Norm* $a_3^{(t)}$ follows the Ftot quenching curve measured simultaneously (Fig. 7). This was verified by fitting an exponential function f(*x*) = *a* + *b* *exp.(−*c**x) to both trends, with the x-axis being time, *a* the steady-state value at *t* = 3 min and *a* + *b* the intercept at *t* = 0 min (Fig. 8). Hence, we demonstrate here a similar
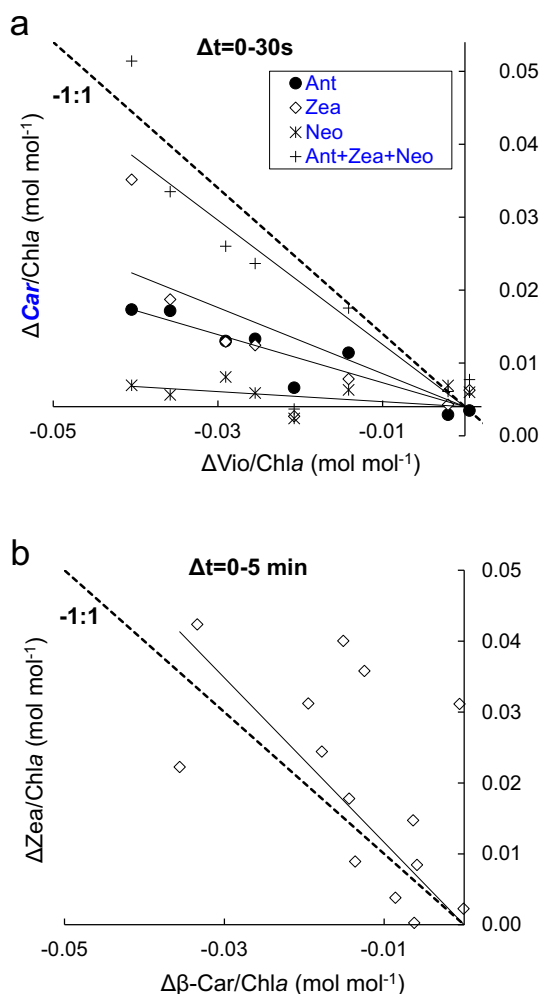
Fig. 6. *Q. robur* ΔCar (Ant, Zea, Neo) changes normalized by Chl*a versus* the ΔVio changes normalized by Chl*a* during the first 30 s and their linear regression fits (Ant: $y = -0.33x$, $R^2 = 0.86$; Zea: $y = -0.45x$, $R^2 = 0.59$; Neo: $y = -0.07x$, $R^2 = 0.44$; Ant + Zea + Neo: $y = -0.85x$, $R^2 = 0.71$) in panel a and the ΔZea/Chl*a* changes *versus* the $\Delta\beta$-Car/Chl*a* changes during the first 5 min upon saturating light (approx. 1600 μmol m^{-2} s^{-1}) ($y = -1.16x$, $R^2 = 0.14$) in panel b.

kinetic behaviour between the Chl*a* F quenching and the underlying GP component behaviour of the absorbance changes in the 500–600 nm region. Further note that we fit here the same function representing the first-order reaction of the Vio de-epoxidation where the slope is defined by the rate constant for Ant and Zea formation (Fig. 5). Such match suggests a parallel kinetic behaviour between the Vio de-epoxidation, the *Norm* $a_3^{(t)}$ behaviour expressing the trend of the underling GP components and the Ftot quenching curve. The latter was verified for the *Q. robur* sample, showing a quick de-epoxidation in the same time frame as the dynamic *in vivo* Chl*a* F quenching (Fig. 9). The dynamic behaviours of *Norm* $a_2^{(t)}$ and *Norm* $a_1^{(t)}$ of all species show moreover strong correspondence with the formation rate and trends expected for respectively Ant and Zea [18]. The increase of the *Norm* $a_2^{(t)}$ trends at 535.4 nm presents similar behaviour as the Ant formation trend, *i.e.* a quick saturation until $t = 30$ s and following decrease. Besides this, the consecutive increase of the *Norm* $a_1^{(t)}$ trends at 513.0 nm follows the slightly delayed Zea formation, with a less steep slope compared to the *Norm* $a_2^{(t)}$. The prominent role of a quick Ant formation which appears from the pigment analyses and is reflected in the behaviour of *Norm* $a_2^{(t)}$ (Fig. 5), indicates a significant Ant contribution in the mechanism. The equal molecular effect of Ant and Zea formation to the quick Vio de-

epoxidation slope during the first 30 s was earlier shown (Fig. 6a). Despite the expectation of an additional F quenching effect of a Lx to Lut pool conversion we could not distinguish an additional underlying spectral component (*e.g.* by an additional GP) for species containing a functional LxL cycle (*F. sylvatica*, *Q. robur*).

4. Discussion

The role of Ant and Zea having a direct (*i.e.* dynamic ^{1}Chl*a** F quenching) and/or an indirect (*i.e.* changing the conformation of the antenna upon their binding, leading to the creation of molecular energy traps) contribution in the energy quenching in the antenna has been under intense examination and controversial discussions over the last decades [10,31,45,47,55–57]. Generally, much attention has been given to Zea, being the most abundant VAZ pigment in the quenched steady-state state of Lhc units, isolated chloroplasts, or leaf samples. Here, based on leaf spectroscopy under a novel set-up involving two spectroradiometers [22] we aimed at better understanding the absorbance dynamics related to the *in vivo* 500–600 nm difference feature at high temporal detail. The advantage of this technique is the possibility to characterize the absorbance transient dynamics as has been shown by dual-wavelength spectrophotometer techniques [29], but combined with the monitoring of the simultaneous *in vivo* transient ^{1}Chl*a** F quenching. The measured F emission (spectrally and hemispherically integrated given in W m^{-2}) under a constant excitation is hereby a direct reflection of the energy distribution within the leaf at the time of photon emission, averaged over 1 s. Under saturating light exposure, the antenna undergoes several biochemical changes meanwhile the lifetime of the emission is quickly decreased during the first minute. Concurrently, we find for all species tested the overall 500–600 nm feature to show a steady-state at $t = 3$ min. Further interesting underlying dynamics are found when applying a constrained fitting strategy based on multiple Gaussians during the 3-min transient. With a minimum of three Gaussians, quick recurring trends in the differential feature can be already distinguished for all cases indicating omnipresent processes. The relative contribution from a quick central GP (535.4 nm in ΔA) and slower GP in the lower-λ tail (513.0 nm in ΔA) show hereby similar kinetics to the expected Ant and Zea formation kinetics described in literature [18,58] and given by the *Q. robur* HPLC analyses (Fig. 5). While VAZ conversion kinetics have been linked to, and modelled by pulse-induced F-based NPQ kinetics [13,58], this is to our knowledge the first time VAZ conversion kinetics are observed in parallel to the quick *in vivo* underlying spectral behaviour in the 500–600 nm range fitting also the kinetics of dynamic F quenching. It indicates that (1) dynamic ^{1}Chl*a** F quenching takes place simultaneously when Ant and Zea are formed in the first minute, and (2) the absorption difference expected from the VAZ conversion is strongly shifted compared to the *in vitro* absorption differences in solution (*cf.* Fig. 1). These two main observations need further careful attention to interpret the spectral behaviour in the 500–600 nm region. The cause of a strong shift in Car absorption behaviour is consistent with a medium-caused electrochromic shift (Stark effect) induced by an increased polarity of the environment of the molecules [59]. Although the exact strength of this effect and its importance on the molecular Car behaviour cannot be quantified *in vivo* [60], the results indicate a remarkable shift with respect to purified pigments in solution (Fig. 1). Apart from this medium-based absorption shift, the kinetic trends of (1) the overall 500–600 nm feature itself, (2) the derived normalized weights of the underlying GP components, and (3) the ^{1}Chl*a** F quenching, allows us to highlight a better mechanistic understanding of the quick photoprotection mechanisms upon excessive light *in vivo*.

The synchronized exponential decrease of the ^{1}Chl*a** fluorescence signal (indicating a decrease in F lifetime) and the normalized weight of the decreasing GP component (accounting for both increasing components) indicate a strong correlation between Ant + Zea formation and ^{1}Chl*a** excitation quenching (Figs. 8, 9). It suggests a close connection and/or coordination between the processes and argues in favour of the
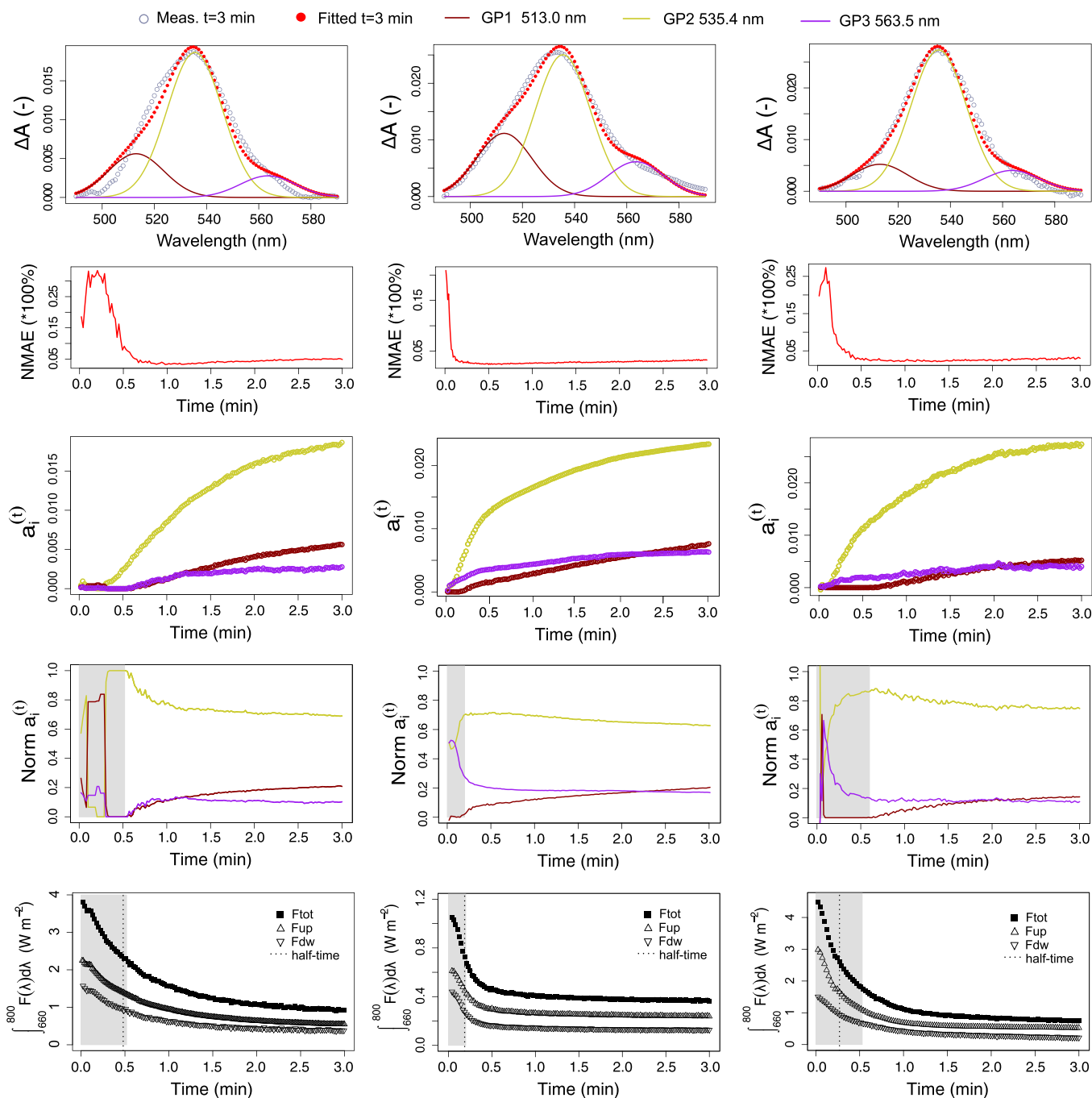
Fig. 7. Final fitting of the 500–600 nm ΔA feature based on three positive GPs at $t = 3$ min for a *M. alba* (left), *F. sylvatica* (middle) and *J. regia* leaf (right). For each transient case the normalized mean absolute error (NMAE) for the fitted feature, the GP weights ($a_i^{(t)}$) and the GP normalized weights (*Norm* $a_i^{(t)}$) during the 3-min feature development are shown, as well as the simultaneous dynamic ^{1}Chl$a$* F quenching measured from the leaf-emitted F spectrally integrated over the [660, 800] nm range in both upward (Fup) and downward (Fdw) direction, and the sum of both (Ftot).

hypothesis that both Ant and Zea act as quencher molecules for ^{1}Chl$a$* states in the antenna. In the context of dynamic quenching a quencher molecule binds to a target and transfers the excitation energy non-radiatively from the donor (a fluorophore) to the acceptor (a quencher) molecule (see the review by [61]). Although a quencher role for the excited ^{1}Chl$a$* molecules has been proposed for both Zea and Lut [29,62], their explicit role in the excited-state energy quenching has been also challenged based on quantum chemical calculations [63] or mutant-based studies [45,57]. We believe, however, that the study of *in vivo* absorption differences in the 500–600 nm region, and more specifically the early-transient phase, may shed new light on the complex

absorption dynamics during the energy-dependent quenching phase.

By probing the kinetic response of Ant and Zea *in vivo* seen by very subtle early-transient absorption changes (see Appendix A, Fig. S2) we can provide a closer look into several distinct kinetic phases during the quick onset of light saturation. Three xanthophyll-related kinetic events can be distinguished from the fitted Gaussians: 1) an instant rise of an Ant-related Gaussian within seconds, followed by 2) a quick rise of a Zea-related Gaussian, both summing the opposite trend of ^{1}Chl$a$* quenching, while 3) a slower absorption mechanism gives a further dominant weight to the Ant-related Gaussian. Generally, the role of Ant with respect to the direct PSII photoprotection mechanism has remained
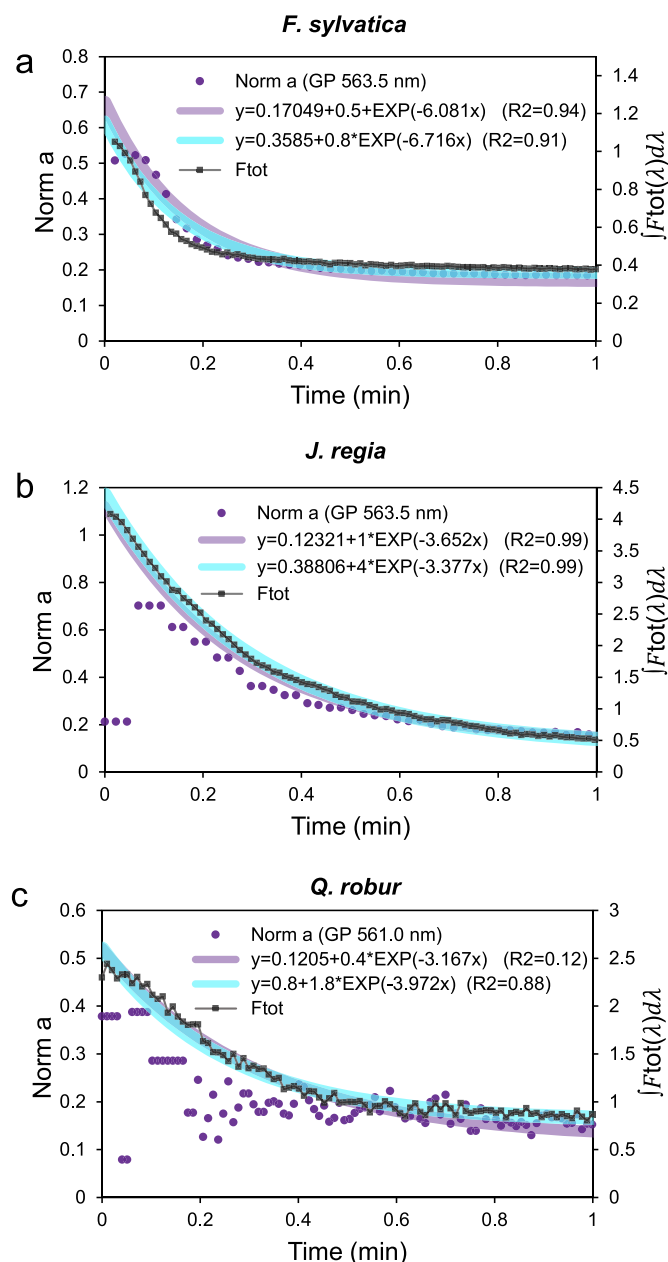
Fig. 9. Violaxanthin pool composition normalized to Chl$a$ (mol mol^{-1}) of *Q. robur* leaves of dark-adapted (black bullets) and Δt-exposed (white bullets) samples during the early stage of the exposure to saturating light ($t = 0$–1 min) in combination with the exponentially fitted Vio de-epoxidation function (blue line) and the [660, 800] nm spectral integral of the leaf-emitted dynamic Chl$a$ Ftot quenching (square-line curve).

Fig. 8. Exponential fittings to the trends of the leaf-emitted dynamic Chl$a$ Ftot quenching spectrally integrated over the [660, 800] nm range and the normalized weight (*Norm $a^{(t)}$*) from the strongest decreasing GP component centred at 563.5 nm (ΔA, Constraints set 1, $N_g = 3$, panel a and b) or 561.0 (ΔR, Constraints set 1, $N_g = 3$, panel c).

undervalued, mainly due to its minor share in the VAZ pool. However, Gilmore and colleagues demonstrated the prominent role of Ant in the ^{1}Chl$a$* quenching based on *in vitro* F lifetime analysis. They indicated two F quenching steps: (1) the pH activation itself or ΔpH-dependent quenching, and (2) the formation of a saturable xanthophyll-PsbS-associated complex that yields a prominent PSII F decay [62] with evidence that Ant was strongly correlated with these F decreases [42,64]. Quick rises in Ant concentration to maximum levels within 1 min or shorter upon light excess have been reported [18,58,65,66], but were not related to specific spectral components in the 500–600 nm region before. The central and dominant Gaussian (*i.e.* at GP2 at 535.4 nm in the simplest ΔA fitting model) alludes a strong relative influence of Ant formation in the early transient phase (Figs. 7, S2), but what is remarkably is the observation of only 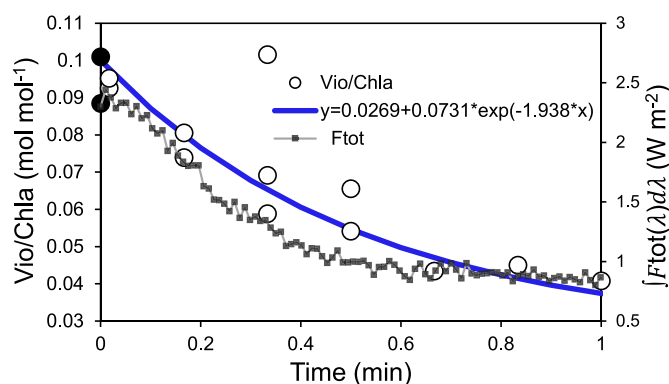as a minor influence in the overall absorbance change by this initial quick rise. The slower and stronger expansion until $t = 3$ min has a larger effect on the total ΔA (Fig. 3). Hence, the slow development of the 500–600 nm feature given by the weight does however *de facto* not match the Ant and Zea formation kinetics, but instead results from a slower increase in the absorption. The findings of these three kinetic phases within the 500–600 nm range stipulate that the quick ΔA increases are not only directly related to the strongly allowed S_0–S_2 electronic transition of these xanthophylls (*i.e.* prompt upon their formation), but also influenced by an additional enhanced absorption process. This enhanced absorption follows the overall lower exponential increase (Fig. 3) where the absorption continues to rise for all GP components until $t = 3$ min but with a dominance of the central GP component (Fig. 7, $a^{(t)}$ trends). The slower exponential increase of the peak around 535 nm observed in earlier studies has been suggested to monitor an allosteric regulation of the pigment-protein complex, acting as a conformational change upon the xanthophyll binding to the antenna during quick energy quenching [29,31]. This cannot be verified by our study, but it is observed that these stronger absorption increases occur from the Ant-related Gaussian. Recently, even further slow absorption increases rising from a 550-nm peak have been dedicated to an additional quenching of excitation energy, involving also a 750-nm peak dedicated to Chl [22]. From all these observations we may suggest a dual working of xanthophylls in the energy quenching process, the first resulting in minor absorption changes but seen in parallel to the dynamic ^{1}Chl$a$* F quenching and the VAZ conversion, and the second mechanism seen as a slower but enhanced absorption mechanism unrelated to the trend of F quenching.

Further, our experiment reveals quick biochemical changes in both α- and β-branch Cars during the sudden light acclimation. Large constitutive differences in the speed of Ant + Zea formation among leaves can be explained by intrinsic and environmental factors, being modulated by the light and temperature conditions during and before the illumination transients. Given that most protocols for cultivation of model plants in growth chambers employ a relatively low PPFD (100–300 μmol m^{-2} s^{-1}) and that experiments of dark-to-strong-light transients usually involve exposure to medium light intensities, or long exposure times, the short-term pigment dynamics upon intense illumination remains largely undetected. β-Car showed here a declining trend upon intense illumination (Figs. 5, 6b). Interestingly, fast *de novo* synthesis of Zea from β-Car has been reported [67] but a rapid conversion within minutes (Fig. 6b) remains unclear. Such a conversion could be hypothesized, although a degradation of β-Car may not be entirely excluded. Also the α-branch Cars show interesting quick dynamics consistent with the fact that the same enzymes are involved in the

β-branch photoconversions [12]. However, these kinetic phases were less clearly observed and could not be additionally derived from the Gaussian decomposition in the 500–600 nm region. Nonetheless, it reveals that all the pigment pools involved in photoprotection are able to convert rapidly to light excess and some photoprotective roles remain to be clarified.

5. Conclusions

In summary, the immediate and mutual increase in leaf absorbance due to specific absorption changes during ^{1}Chl$a$* F quenching measured from a dual spectroradiometer set-up allows the observation of consistent changes in the diffuse leaf surface scattering originating from the interior elements. While slower chloroplast movement may potentially affect the scattering behaviour in this region as well, a bell-shaped specific absorption feature is generally clearly distinguished, characterized by a quick exponential increase of all 500–600 nm wavelengths during a 3-min dark-to-high-light transient. Describing this feature by the presented fitting of multiple Gaussians demonstrated an easy and effective method to reveal underlying spectral behaviour which we could kinetically relate to the ubiquitous plant VAZ cycle operating at the early stage of the transient. The underlying Gaussian components found by this technique indicated simultaneous kinetic trends of two absorption mechanisms in parallel with the dynamic ^{1}Chl$a$* F quenching under constant illumination. Moreover, the kinetic behaviour of these underlying component trends matched the parallel behaviour of the dynamic ^{1}Chl$a$* F quenching and the formation dynamics of both Ant and Zea ($t = 0$–1 min). A slower enhanced absorption of the overall feature dominated by the Ant-related Gaussian at 535 nm does not contribute to any further ^{1}Chl$a$* F quenching and points to an increased absorption controlled by a slower mechanism. We believe these observations contribute to new insights into the complex energy excitation distribution and relaxation mechanisms within the light reactions, suggesting a role for both Ant and Zea as quencher molecules. The operation of these pigments is observed under a strong red-shifted absorption until the 500–600 nm region where absorption changes are altered averagely by 2–3%. Future experiments should further contribute to an improved mechanistic understanding of the *in vivo* xanthophyll spectral behaviour in this region, as it highlights a potential for the remote monitoring of the non-photochemical energy dissipation dynamics of absorbed light by vegetation.

CRediT authorship contribution statement

SVW designed the dual spectrometer set-up, collected the spectral and pigment data, performed the spectral fitting analysis together with VL and interpreted the results under the guidance and advice of JM. JIGP and BFM performed the HPLC analysis and helped with the further interpretation of the results. VL, JIGP, BFM and APC assisted with the preparation of the manuscript.

Declaration of competing interest

The authors declare that they have no conflict of interest.

Acknowledgements

Appendix A. Supplementary data

Supplementary data to this article can be found online at https://doi.org/10.1016/j.bbabio.2020.148351.

References

[1] G.D. Scholes, G.R. Fleming, A. Olaya-Castro, R. van Grondelle, Lessons from nature about solar light harvesting, Nat. Chem. 3 (2011) 763–774.

[2] A.A. Pascal, Z. Liu, K. Broess, B. Van Oort, H. Van Amerongen, C. Wang, P. Horton, B. Robert, W. Chang, A. Ruban, Molecular basis of photoprotection and control of photosynthetic light-harvesting, Nature 436 (2005) 134–137.

[3] J. Zhou, S. Sekatskii, R. Welc, G. Dietler, W. Gruszecki, The role of xanthophylls in the supramolecular organization of the photosynthetic complex LHCII in lipid membranes studied by high- resolution imaging and nanospectroscopy, BBA-Bioenergetics 148117 (2020).

[4] J. Peñuelas, I. Filella, J. Gamon, Assessment of photosynthetic radiation use efficiency with spectral reflectance, New Phytol. (1995) 291–296.

[5] C.Y.S. Wong, J.A. Gamon, The photochemical reflectance index provides an optical indicator of spring photosynthetic activation in evergreen conifers, New Phytol. 206 (2015) 196–208.

[6] T. Mirkovic, E.E. Ostroumov, J.M. Anna, R. van Grondelle, Govindjee, G. D. Scholes, Light absorption and energy transfer in the antenna complexes of photosynthetic organisms, Chem. Rev. 117 (2017) 249–293.

[7] T.P.J. Krüger, R. van Grondelle, The role of energy losses in photosynthetic light harvesting, J. Phys. B Atomic Mol. Phys. 50 (2017) 132001.

[8] Z. Liu, H. Yan, K. Wang, T. Kuang, J. Zhang, L. Gui, X. An, W. Chang, Crystal structure of spinach major light-harvesting complex at 272 Å resolution, Nature 428 (2004) 287–292.

[9] M. Durchan, G. Keşan, V. Šlouf, M. Fuciman, H. Staleva, J. Tichý, R. Litvín, D. Bína, F. Vácha, T. Polívka, Highly efficient energy transfer from a carbonyl carotenoid to chlorophyll a in the main light harvesting complex of Chromera velia, Biochim. Biophys. Acta Bioenerg. 1837 (2014) 1748–1755.

[10] R. Welc, R. Luchowski, W. Grudzinski, M. Puzio, K. Sowinski, W.I. Gruszecki, A key role of xanthophylls that are not embedded in proteins in regulation of the photosynthetic antenna function in plants, revealed by monomolecular layer studies, J. Phys. Chem. B 120 (2016) 13056–13062.

[11] B. Demmig-Adams, Carotenoids and photoprotection in plants: a role for the xanthophyll zeaxanthin, Biochim. Biophys. Acta 1020 (1990) 1–24.

[12] J.I. García-Plazaola, S. Matsubara, C.B. Osmond, The lutein epoxide cycle in higher plants: its relationships to other xanthophyll cycles and possible functions, Funct. Plant Biol. 34 (2007) 759–773.

[13] M. Leuenberger, J.M. Morris, A.M. Chan, L. Leonelli, K.K. Niyogi, G.R. Fleming, Dissecting and modeling zeaxanthin- and lutein-dependent nonphotochemical quenching in Arabidopsis thaliana, Proc. Natl. Acad. Sci. U. S. A. 114 (2017) E7009–E7017.

[14] B. Förster, B.J. Pogson, C.B. Osmond, Lutein from deepoxidation of lutein epoxide replaces zeaxanthin to sustain an enhanced capacity for nonphotochemical chlorophyll fluorescence quenching in avocado shade leaves in the dark, Plant Physiol. 156 (2011) 393–403.

[15] C. Ilioaia, M.P. Johnson, C.D.P. Duffy, A.A. Pascal, R. Van Grondelle, B. Robert, A. V. Ruban, Origin of absorption changes associated with photoprotective energy dissipation in the absence of zeaxanthin, J. Biol. Chem. 286 (2011) 91–98.

[16] W. Bilger, O. Bjorkman, S.S. Thayer, Light-induced spectral absorbance changes in relation to photosynthesis and the epoxidation state of xanthophyll cycle components in cotton leaves, Plant Physiol. 91 (1989) 542–551.

[17] A.V. Ruban, R. Berera, C. Ilioaia, I.H.M. Van Stokkum, J.T.M. Kennis, A.A. Pascal, H. Van Amerongen, B. Robert, P. Horton, R. van Grondelle, Identification of a mechanism of photoprotective energy dissipation in higher plants, Nature 450 (2007) 575–579.

[18] J.J. Peguero-Pina, E. Gil-Pelegrín, F. Morales, Three pools of zeaxanthin in Quercus coccifera leaves during light transitions with different roles in rapidly reversible photoprotective energy dissipation and photoprotection, J. Exp. Bot. 64 (2013) 1649–1661.

[19] R. Croce, S. Weiss, R. Bassi, Carotenoid-binding sites of the major light-harvesting complex II of higher plants carotenoid-binding sites of the major light-harvesting complex II of higher plants, J. Biol. Chem. 274 (1999) 29613–29623.

[20] E. Brugnoli, O. Björkman, Chloroplast movements in leaves: influence on chlorophyll fluorescence and measurements of light-induced absorbance changes related to ΔpH and zeaxanthin formation, Photosynth. Res. 32 (1992) 23–35.

[21] G. Garab, Hierarchical organization and structural flexibility of thylakoid membranes, Biochim. Biophys. Acta Bioenerg. 1837 (2014) 481–494.

[22] S. Van Wittenberghe, L. Alonso, Z. Malenovský, J. Moreno, In vivo photoprotection mechanisms observed from leaf spectral absorbance changes showing VIS–NIR slow-induced conformational pigment bed changes, Photosynth. Res. 142 (2019) 283–305.

[23] G. Allorent, M. Byrdin, L. Carraretto, T. Morosinotto, I. Szabo, G. Finazzi, Global spectroscopic analysis to study the regulation of the photosynthetic proton motive force: a critical reappraisal, Biochim. Biophys. Acta Bioenerg. 1859 (2018) 676–683.

[24] S. Viola, B. Bailleul, J. Yu, P. Nixon, J. Sellés, P. Joliot, F.A. Wollman, Probing the electric field across thylakoid membranes in cyanobacteria, Proc. Natl. Acad. Sci. U. S. A. 116 (2019) 21900–21906.

[25] B. Bailleul, P. Cardol, C. Breyton, G. Finazzi, Electrochromism: a useful probe to study algal photosynthesis, Photosynth. Res. 106 (2010) 179–189.

[26] T. Polívka, V. Sundström, Dark excited states of carotenoids: consensus and controversy, Chem. Phys. Lett. 477 (2009) 1–11.

[27] L. Dall'Osto, N.E. Holt, S. Kaligotla, M. Fuciman, S. Cazzaniga, D. Carbonera, H. A. Frank, J. Alric, R. Bassi, Zeaxanthin protects plant photosynthesis by modulating chlorophyll triplet yield in specific light-harvesting antenna, J. Biol. Chem. 287 (2012) 41820–41834.

[28] E.J.G. Peterman, R. Monshouwer, I.H.M. Van Stokkum, R. van Grondelle, H. Van Amerongen, Ultrafast singlet excitation transfer from carotenoids to chlorophylls via different pathways in light-harvesting complex II of higher plants, Chem. Phys. Lett. 264 (1997) 279–284.

[29] M.P. Johnson, M.L. Pérez-Bueno, A. Zia, P. Horton, A.V. Ruban, The zeaxanthin-independent and zeaxanthin-dependent qE components of nonphotochemical quenching involve common conformational changes within the photosystem II antenna in Arabidopsis, Plant Physiol. 149 (2009) 1061–1075.

[30] A.V. Ruban, J. Young, P. Horton, Induction of nonphotochemical energy dissipation and absorbance changes in leaves (evidence for changes in the state of the light-harvesting system of photosystem II in vivo), Plant Physiol. 102 (1993) 741–750.

[31] P. Horton, A.V. Ruban, M. Wentworth, Allosteric regulation of the light-harvesting system of photosystem II, Philos. Trans. Biol. Sci. 355 (2000) 1361–1370.

[32] W. Bilger, O. Björkman, Role of the xanthophyll cycle in photoprotection elucidated by measurements of light-induced absorbance changes, fluorescence and photosynthesis in leaves of Hedera canariensis, Photosynth. Res. 25 (1990) 173–185.

[33] J.A. Gamon, C.B. Field, O.W. Bilger, Björkman, A.L. Fredeen, J. Peñuelas, Remote sensing of the xanthophyll cycle and chlorophyll fluorescence in sunflower leaves and canopies, Oecologia 85 (1990) 1–7.

[34] D. Kovác, Z. Malenoský, O. Urban, V. Špunda, A. Alexander, V. Kaplan, J. Hanuš, Response of green reflectance continuum removal index to the xanthophyll de-epoxidation cycle in Norway spruce needles, J. Exp. Bot. 64 (2013) 1817–1827.

[35] K. Acebron, S. Matsubara, C. Jedmowski, D. Emin, O. Muller, U. Rascher, Diurnal dynamics of non-photochemical quenching in Arabidopsis npq mutants assessed by solar-induced fluorescence and reflectance measurements in the field, New Phytol. (2020), https://doi.org/10.1111/nph.16984.

[36] Y. Inoue, K. Shibata, Light-induced chloroplast rearrangements and their action spectra as measured by absorption spectrophotometry, Planta 114 (1973) 341–358.

[37] J.A. Gamon, J.S. Surfus, Assessing leaf pigment content and activity with a reflectometer, New Phytol. 143 (1999) 105–117.

[38] A. Gamon, L. Serrano, S. Surfus, The photochemical reflectance index: an optical indicator of photosynthetic radiation use efficiency across species, functional types, and nutrient levels, Oecologia (1997) 492–501.

[39] E. Sukhova, V. Sukhov, Relation of photochemical reflectance indices based on different wavelengths to the parameters of light reactions in photosystems I and II in pea plants, Remote Sens. 1312 (2020).

[40] P. Rahimzadeh-Bajgiran, M. Munehiro, K. Omasa, Relationships between the photochemical reflectance index (PRI) and chlorophyll fluorescence parameters and plant pigment indices at different leaf growth stages, Photosynth. Res. 113 (2012) 261–271.

[41] C.D.P. Duffy, J. Chmeliov, M. Macernis, J. Sulskus, L. Valkunas, A.V. Ruban, Modeling of fluorescence quenching by lutein in the plant light-harvesting complex LHCII, J. Phys. Chem. B 117 (2013) 10974–10986.

[42] A.M. Gilmore, H.Y. Yamamoto, Time-resolution of the antheraxanthin- and ΔpH-dependent chlorophyll a fluorescence components associated with photosystem II energy dissipation in Mantoniella squamata, Photochem. Photobiol. 74 (2001) 291.

[43] P. Horton, A.V. Ruban, R.G. Walters, Regulation of light harvesting in green plants, Annu. Rev. Plant Physiol. Plant Mol. Biol. 47 (1996) 655–684.

[44] D. Gacek, C. Peter, H. Pen, N. Liao, M. Negretti, R. Croce, P. Walla, Carotenoid dark state to chlorophyll energy transfer in isolated light - harvesting complexes CP24 and CP29, Photosynth. Res. (2020) 19–30.

[45] P. Xu, L. Tian, M. Kloz, R. Croce, Molecular insights into Zeaxanthin-dependent quenching in higher plants, Sci. Rep. 5 (2015) 1–10.

[46] B. Van Oort, L.M. Roy, P. Xu, Y. Lu, D. Karcher, R. Bock, R. Croce, Revisiting the role of xanthophylls in nonphotochemical quenching, J. Phys. Chem. Lett. 9 (2018) 346–352.

[47] M.G. Müller, P. Lambrev, M. Reus, E. Wientjes, R. Croce, A.R. Holzwarth, Singlet energy dissipation in the photosystem II light-harvesting complex does not involve energy transfer to carotenoids, ChemPhysChem 11 (2010) 1289–1296.

[48] L. Alonso, S. Van Wittenberghe, J. Amorós-López, J. Vila-Francés, L. Gomez-Chova, J. Moreno, Diurnal cycle relationships between passive fluorescence, PRI and NPQ of vegetation in a controlled stress experiment, Remote Sens. 9 (2017) 1–16.

[49] L. Alonso, L. Gómez-Chova, J. Vila-Francés, J. Amorós-López, J. Guanter, L. Calpe, J. Moreno, Sensitivity analysis of the Fraunhofer line discrimination method for the measurement of chlorophyll fluorescence using a field spectroradiometer, in: Proc. 3th Int. Work. Remote Sens. Veg. Fluoresc., Florence, 2007, pp. 3756–3759.

[50] S. Van Wittenberghe, L. Alonso, J. Verrelst, I. Hermans, J. Delegido, F. Veroustraete, R. Valcke, J. Moreno, R. Samson, Upward and downward solar-induced chlorophyll fluorescence yield indices of four tree species as indicators of traffic pollution in Valencia, Environ. Pollut. 173 (2013) 29–37.

[51] J.I. García-Plazaola, A. Hernández, E. Errast, J.M. Becerril, Occurence and operation of the lutein epoxide cycle in Quercus species, Funct. Plant Biol. 29 (2002) 1075–1080.

[52] J.I. García-Plazaola, J.M. Becerril, A rapid high-performance liquid chromatography method to measure lipophilic antioxidants in stressed plants: simultaneous determination of carotenoids and tocopherols, Phytochem. Anal. 10 (1999) 307–313.

[53] H. Küpper, M. Spiller, F.C. Küpper, Photometric method for the quantification of chlorophylls and their derivatives in complex mixtures: fitting with Gauss-peak spectra, Anal. Biochem. 256 (2000) 247–256.

[54] H. Küpper, S. Seibert, A. Parameswaran, Fast, sensitive, and inexpensive alternative to analytical pigment HPLC: quantification of chlorophylls and carotenoids in crude extracts by fitting with Gauss peak spectra, Anal. Chem. 79 (2007) 7611–7627.

[55] C. Ilioaia, M. Johnson, P.-N. Liao, A. Pascal, R. van Grondelle, P. Walla, A. Ruban, B. Robert, Photoprotection in plants involves a change in lutein 1 binding domain in the major light-harvesting complex of photosystem II, J. Biol. Chem. (2011) 27247–27254.

[56] A.V. Ruban, R.G. Walters, P. Horton, The molecular mechanism of the control of excitation energy dissipation in chloroplast membranes inhibition of delta pH-dependent quenching of chlorophyll fluorescence by dicyclohexylcarbodiimide, FEBS Lett. 309 (1992) 175–179.

[57] L. Tian, P. Xu, V.U. Chukhutsina, A.R. Holzwarth, R. Croce, Zeaxanthin-dependent nonphotochemical quenching does not occur in photosystem I in the higher plant Arabidopsis thaliana, Proc. Natl. Acad. Sci. U. S. A. 114 (2017) 4828–4832.

[58] D. Latowski, K. Burda, K. Strzałka, A mathematical model describing kinetics of conversion of violaxanthin to zeaxanthin via intermediate antheraxanthin by the xanthophyll cycle enzyme violaxanthin de-epoxidase, J. Theor. Biol. 206 (2000) 507–514.

[59] H.A. Frank, J.A. Bautista, J. Josue, Z. Pendon, R.G. Hiller, F.P. Sharples, D. Gosztola, M.R. Wasielewski, Effect of the solvent environment on the spectroscopic properties and dynamics of the lowest excited states of carotenoids, J. Phys. Chem. B 104 (2000) 4569–4577.

[60] S. Krawczyk, R. Luchowski, Vibronic structure and coupling of higher excited electronic states in carotenoids, Chem. Phys. Lett. 564 (2013) 83–87.

[61] L. Cupellini, M. Corbella, B. Mennucci, C. Curutchet, Electronic energy transfer in biomacromolecules, Wiley Interdiscip. Rev. Comput. Mol. Sci. 9 (2019) 1–23.

[62] A.M. Gilmore, T.L. Hazlett, Govindjee, Xanthophyll cycle-dependent quenching of photosystem II chlorophyll a fluorescence: formation of a quenching complex with a short fluorescence lifetime, Proc. Natl. Acad. Sci. U. S. A. 92 (1995) 2273–2277.

[63] A. Dreuw, M. Wormit, Simple replacement of violaxanthin by zeaxanthin in LHC-II does not cause chlorophyll fluorescence quenching, J. Inorg. Biochem. 102 (2008) 458–465.

[64] A.M. Gilmore, H.Y. Yamamoto, Linear models relating xanthophylls and lumen acidity to non-photochemical fluorescence quenching evidence that antheraxanthin explains zeaxanthin-independent quenching, Photosynth. Res. 35 (1993) 67–78.

[65] S. Heyde, P. Jahns, The kinetics of zeaxanthin formation is retarded by dicyclohexylcarbodiimide, Plant Physiol. 117 (1998) 659–665.

[66] K.M. Sun, C. Gao, J. Zhang, X. Tang, Z. Wang, X. Zhang, Y. Li, Rapid formation of antheraxanthin and zeaxanthin in seconds in microalgae and its relation to non-photochemical quenching, Photosynth. Res. 144 (2020) 317–326.

[67] B. Depka, P. Jahns, A. Trebst, β-Carotene to zeaxanthin conversion in the rapid turnover of the D1 protein of photosystem II, FEBS Lett. 424 (1998) 267–270.